Journal of Materials Chemistry A

Accepted Manuscript

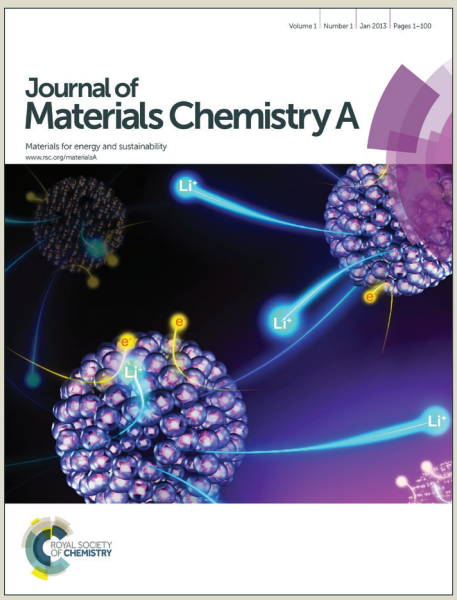

This is an *Accepted Manuscript*, which has been through the Royal Society of Chemistry peer review process and has been accepted for publication.

Accepted Manuscripts are published online shortly after acceptance, before technical editing, formatting and proof reading. Using this free service, authors can make their results available to the community, in citable form, before we publish the edited article. We will replace this *Accepted Manuscript* with the edited and formatted *Advance Article* as soon as it is available.

You can find more information about *Accepted Manuscripts* in the Information for Authors.

Please note that technical editing may introduce minor changes to the text and/or graphics, which may alter content. The journal's standard Terms & Conditions and the Ethical guidelines still apply. In no event shall the Royal Society of Chemistry be held responsible for any errors or omissions in this *Accepted Manuscript* or any consequences arising from the use of any information it contains.

ROYAL SOCIETY OF CHEMISTRY

www.rsc.org/materialsA

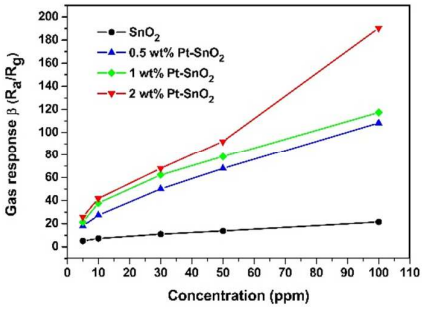

Pt-functionalized SnO_2 sheets based gas sensor displayed a response value of 190.5 for 100 ppm isopropanol gas.

Journal of Materials Chemistry A Accepted Manuscript

Journal Name

RSCPublishing

ARTICLE

Combustion synthesis of porous Pt-functionalized SnO_2 sheets for isopropanol gas detection with a significant enhancement in response

Cite this: DOI: 10.1039/xoxxoooooox

Received ooth January 2012,
Accepted ooth January 2012

DOI: 10.1039/xoxxoooooox

www.rsc.org/

Chengjun Dong,[a] Xu Liu,[a] Xuechun Xiao,[a] Gang Chen,[a] Yude Wang,*[a] and Igor Djerdj*[b]

Pt-functionalized SnO_2 sheets with Pt contents of 0, 0.5, 1, and 2 wt% were synthesized by a facile solution combustion synthesis, and their crystal structure, morphology, and chemistry have been thoroughly characterized. In the combustion process, the urea ($CO(NH_2)_2$) has been employed as a fuel. The obtained products appear as porous sheets formed by the interconnected and loosely packed SnO_2 nanoparticles. Pt nanoparticles are assembled together with SnO_2 nanoparticles in several up to tens of nanometers clusters. The as-synthesized products were used as sensing materials in the sensors to detect isopropanol (IPA) gas. Gas sensing tests exhibited that the Pt-functionalized SnO_2 are highly promising for gas sensor applications, as the operating temperature was lower than current IPA sensors and the response to IPA was significantly enhanced. The 2 wt% Pt-SnO_2 sheets based gas sensor displayed a response value of 190.50 for 100 ppm IPA at optimized operating temperature of 220 °C, whereas the pristine SnO_2 based gas sensor only showed a response of 21.53 under the same conditions. The role of Pt nanoparticles on electronic sensitization of SnO_2, catalytic oxidation (spillover effect), and the increased quantities of oxygen species on the surface of SnO_2, are plausible reasons to explain the significant enhancement in response for Pt-functionalized SnO_2 sheets based gas sensor.

1. Introduction

As we know, toxic or explosive volatile organic compounds (VOCs), such as IPA, acetone, formaldehyde, methanol, ethanol, etc, are seriously harmful to both humans and the environment.[1] In particular, IPA (also known as 2-propanol, isopropyl alcohol) is a colourless transparent liquid with slightly bitter taste, which has been widely used in solvents, pharmaceuticals, cosmetics, disinfectants, lubricants, and other aspects of living. However, IPA can decompose to a poisonous gas under high temperature and easily spreads to a distance, posing harmful effects to human health. It is reported that IPA gas can cause a mild irritation of the human upper respiratory tract and discomfort of the eyes even below the concentration of 400 ppm, while a higher concentration can inhibit the central nervous system, leading to dizziness, severe vomiting, decreased respiration, excessive sweating, swelling, and internal bleeding.[2] Therefore, detection of IPA vapour is of great importance in terms of human health and environmental safety. Nowadays, gas chromatography and mass spectrometry are common options among the available techniques for VOCs detection. However, these methods are limited by their high cost, complex fabrication process, large size, and inability to perform *in situ* and continuous measurements. Fortunately, semiconductor metal oxide gas sensors provide a promising alternative for monitoring of VOCs and detection due to their good sensing capabilities and the fact that they can be easily mass-produced.

SnO_2, an n-type semiconductor with a wide band gap of 3.62 eV, is one of the most interesting prospects because of its high chemical stability and excellent optical and electrical properties. Apart from the applications in catalysts, lithium rechargeable batteries, optical electronic devices, and so on, it has especially been used as a gas sensing material for detection of various VOCs due to its low cost, high sensitivity, and fast gas response.[3] Hence, a number of chemical and physical approaches have been developed to fabricate diverse SnO_2 sensors, for instance, hydrothermal,[4] chemical vapour deposition,[5] molten-salt method,[6] electrospinning,[7] just name a few. Nevertheless, finding a novel approach with the advantages of simplicity, low cost, and time saving to synthesize porous SnO_2 sheets for gas sensors is still of great technological and scientific interest. Solution combustion synthesis offers an effective, rapid and energy-efficient method for productions of various nanomaterials in large scale. It is based on an extremely rapid

Journal of Materials Chemistry A Accepted Manuscript

exothermic reaction between an oxidizer (metal nitrates) and an organic fuel (such as citric acid, glycine, urea or ethylene glycol) in just a few minutes. A characteristic feature of this method is that combustion synthesis supplies a localized energy by self-generated heat to drive the chemical reaction, eliminating the continuous requirement for a high external processing temperature.[8,9] As a result, many functional materials such as ZnO,[10] In_2O_3,[11] NiO,[12] have been recently fabricated by means of the combustion route. A little work has been focused on combustion synthesized SnO_2 nanostructures. Kang *et al.* synthesized the SnO_2:Eu^{3+} phosphor by an optimized combustion method varying the molar ratio of citric acid to HNO_3 as a process parameter.[13] As the fuel choice is a critical factor for combustion synthesis, it is highly worthwhile to attempt to use a novel fuel such as urea in the synthesis of SnO_2 for gas sensors. Moreover, to improve the gas sensing performances of SnO_2 based gas sensors, the SnO_2 is functionalized and tuned by catalytic noble metals, especially Pt. Jang and co-workers synthesized SnO_2 nanofibers functionalized by Pt nanoparticles for the sensitive and selective detection of H_2 and NO_2 gases in the presence of NH_3, CO and SO_2.[14] Kocemba *et al.* discussed the influence of catalytic activity on the response of Pt/SnO_2 gas sensors to carbon monoxide and hydrogen.[15] Xu's research group reported the synthesis of uniformly loaded Pt@SnO_2 nanorods for highly sensitive gas sensors for ethanol by a one-step hydrothermal route.[16] However, to our best knowledge, few works have dealt with SnO_2 based IPA gas sensors. Moreover, the sensing properties of IPA on the Pt-functionalized SnO_2 base synthesized by solution combustion synthesis are still unknown.

In this article, we report a facile solution combustion method to fabricate Pt-functionalized SnO_2 with Pt contents of 0, 0.5, 1, and 2 wt% using urea as a fuel. The porous Pt-functionalized SnO_2 sheets were directly formed at a low temperature of 400 °C in a short time of 30 min. First, the phase structures, morphologies, compositions, chemical states, and microstructures of as-synthesized products have been thoroughly investigated. To demonstrate the potential applications, we have constructed gas sensors based on as-synthesized Pt-functionalized SnO_2 products and comparably investigated their gas-sensing properties using IPA as a target gas. The obtained results indicate that the gas sensor based on the Pt-functionalized SnO_2, especially with Pt content of 2 wt%, exhibited a significant enhancement in response and a lower operating temperature than that of pristine SnO_2.

2. Experimental

2.1. Materials

All chemicals including tin (II) chloride dihydrate ($SnCl_2$•$2H_2O$), nitric acid (HNO_3, 68%), urea ($CO(NH_2)_2$), (hydro) chloroplatinic acid (H_2PtCl_6•$6H_2O$) and IPA were purchased from commercial sources. The chemicals were analytical grade reagents and used as received without any further purification. Milli-Q water (resistivity of 18 MΩ•cm at 25 °C) was used throughout all experiments.

2.2. Synthesis of porous Pt-functionalized SnO_2 sheets

The pristine SnO_2 and Pt-functionalized SnO_2 were synthesized by a facial solution combustion method. In a previous report, Kang and co-workers synthesized SnO_2 via an optimized combustion method by varying the molar ratio of citric acid to HNO_3.[13] Here we used substitued citric acid with urea by modifying their reaction to provide a novel option. The stoichiometric composition of the oxidizer and fuel are calculated upon the complete combustion reaction below:

$$SnCl_2 \cdot 2H_2O + 4.5\ CO(NH_2)_2 + 6.2HNO_3 \rightarrow SnO_2 + Cl_2 + 7.6N_2 + 4.5\ CO_2 + 14.1\ H_2O \quad (1)$$

In a typical synthesis procedure of pristine SnO_2, 12.4 mM HNO_3 (68%) was first dissolved in 10 ml deionized water. Afterwards, 2 mM $SnCl_2$•$2H_2O$ was completely dissolved into the above solution under vigorous magnetic stirring for 30 min. Then 9 mM $CO(NH_2)_2$ was added into the solution to get a clean combustion precursor. Subsequently, this combustion precursor was transferred into a quartz crucible, and put into a preheated furnace maintained at 400 °C. Within a few minutes, the precursor solution boiled and ignited in self-propagating combustion. After a total of 30 minutes, the crucible was taken out and cooled in atmospheric conditions. The crucible was filled with fluffy loose products. In the case of Pt-functionalized SnO_2, the solution preparation and experimental procedure were similar except that the corresponding amount of H_2PtCl_6•$6H_2O$ was added after the $SnCl_2$•$2H_2O$. Finally, porous products were collected for gas sensor fabrication. For clarity, Fig. S1 (Supp. Inf.) schematically shows the preparation of porous SnO_2 sheets by a solution combustion synthesis and the assembling of the sensor.

2.3. Characterization

The phase identification was made by X-ray diffraction (XRD, Rigaku TTRIII) with an incident X-ray wavelength of 1.54056 Å (CuKα line). All the measurements were performed in the 2θ range 10-80° in steps of 0.02°. The scanning electron microscope (SEM) images of the products were taken using a FEI QUANTA 200 with an attached EDX detector at an accelerating voltage of 30 kV. The transmission electron microscope (TEM) images, selected-area area diffraction (SAED) patterns, and high-resolution transmission electron microscope (HRTEM) images were examined on a JEOL JEM-2100) with an acceleration voltage of 200 kV. X-ray photoelectron spectroscopy (XPS) was recorded in ESCALAB system with AlKα X-ray radiation at 15 kV. All XPS spectra were accurately calibrated by C 1s peak at 284.6 eV to compensate for the charge effect. An American TA SDT-2960 thermal analyzer was utilized to analyze the thermal decomposition of the dried combustion precursor in air. The specific surface areas of the samples have been checked by N_2 adsorption-desorption isotherm with a Micrometrics Autopore IV 9500 system and further calculated by Brunauer-Emmett-Teller (BET) method.

2.4. Fabrication and measurement of IPA gas sensors using obtained products

The gas sensors were fabricated with as-synthesized Pt-functionalized SnO_2 with different Pt contents (0, 0.5, 1 and 2 wt%) as sensing materials. In order to measure the response to IPA,sensors were constructed as follows. The as-synthesized products were mixed with an appropriate volume of deionized water to form a paste. Then the paste was coated by a paint pen onto the outside surface of an alumina tube with a pair of Au electrodes and corresponding platinum wires installed at each end. The alumina tubes are 4 mm in length, 1.2 mm in external diameter, and 0.8 mm in internal diameter. Note that the coating should be uniform and cover the whole of the Au electrodes completely to make a good contact. The tube with coated gas sensing materials was calcined in air at 400 °C for 1 hour and then a Ni-Cr heating wire was inserted in the tube to control the operating temperature by a heating voltage. As illustrated in Fig.

Journal of Materials Chemistry A Accepted Manuscript

 This journal is © The Royal Society of Chemistry 2012

S1, the coated tube and heating wire were well connected to Bakelite base through platinum wires to perform electrical measurements. To improve their stability and repeatability, the gas sensors were aged at 350 °C in dry air before measuring the gas sensing properties using a WS-30A system (Weisheng Instruments Co. Zhengzhou, China). When the resistances of all the sensors were stable, the desired amounts of IPA solution were injected into the chamber (18 L in volume) by a microsyringe. The solution was evaporated by a quick evaporator and mixed with air immediately by two fans installed in the chamber. The values of sensor resistance and dynamic responses were recorded by the analysis system automatically. As a typical n-type gas sensor, its response (β) was defined as the ratio (R_a/R_g) of the sensor resistance in dry air (R_a) to that of analyte gas (R_g). The sensors were examined in the temperature range of 200 to 300 °C at various concentrations of IPA (5-100 ppm).

3. Results and discussion

To investigate the influence of Pt functionalization on SnO_2, XRD analysis was carried out. By comparing the measured XRD pattern with standard pattern of JCPDS: 04-0802 (Pt phase) and JCPDS: 41-1445 (SnO_2 phase), the crystal structure information is obtained. As can be seen in Fig. 1, the main diffraction peaks are perfectly in line with the rutile SnO_2 phase and maintained after Pt functionalization. No Pt related peaks are found in 0.5 wt% Pt-SnO_2 due to its small content. In contrast, for higher Pt functionalization (1 wt% and 2 wt%) two additional peaks located at 39.76°, and 46.28° fit well with (111) and (200) reflections of Pt. Taking a closer look, the Pt related diffraction peaks increase with the increase of Pt contents from 1 wt% to 2 wt%, suggesting that crystalline Pt nanoparticles are independent of SnO_2. Moreover, no other visible peaks such as PtO or PtO_2 diffraction peaks are found in the XRD patterns of Pt-functionalized SnO_2. These results confirm the successful synthesis of Pt-functionalized SnO_2 via a solution combustion method using $CO(NH_2)_2$ as a fuel. The average grain size is estimated to be approximate 10 nm regardless Pt loading level using Scherrer equation derived from the XRD results.

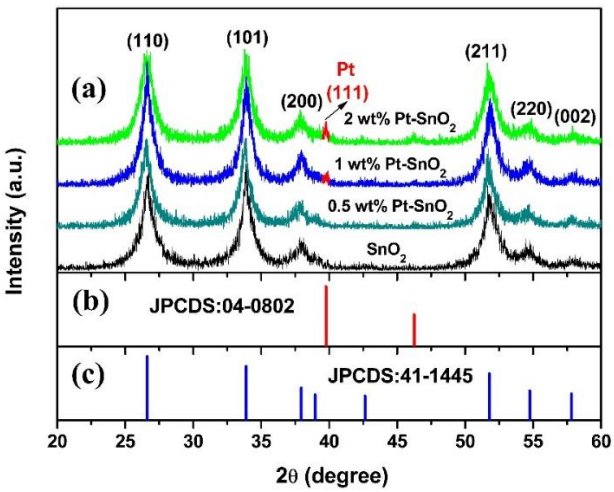

Fig. 1 XRD patterns of (a) different contents (0, 0.5, 1 and 2 wt%) of Pt-functionalized SnO_2, (b) JCPDS:04-0802 of Pt phase, and (c) JCPDS:41-1445 of SnO_2 phase.

The morphology and the microstructure of the pristine SnO_2 particles/ sheets are characterized by SEM, as displayed in Fig. 2. The SEM images in Fig. 2 (a, b) depict both featured inner- and outer-sides of the SnO_2. The pristine SnO_2 appears to have an uneven shell in terms of shape. Generally, the combusted products come out porous and foamy due to the rapid release of gaseous byproducts such as CO_2, CO and H_2O during the combustion reaction.[17] Unlike the reported combusted products, many bumps or bubbles originated from the swelling of gaseous liberation instead of a large number of pores. This is probably attributed to the mild reaction by a fuel of $CO(NH_2)_2$. In addition, the SnO_2 shell is comprised of subunits of smooth sheets, as supported by the high-magnification SEM in Fig. 2 (c), which will be further investigated by the following TEM measurement.

A simultaneous TGA and DSC analysis has been performed to understand the combustion process for the formation of pristine SnO_2 at a heating rate of 10 °C/min from room temperature to 800 °C in air. The combustion precursor was dried at 80 °C and then was used for the thermal measurement, as plotted in Fig. 2(d). The first peak in the DSC curves represents an endothermic peak at 154.83 °C accompanied by a weight loss of about 10%, corresponding to the loss of adsorbed and residual water. The second weight loss of 18% takes place in the temperature range from 158 to 185 °C. This involves the decomposition of organic parts into CO_2 and H_2O vapour, which is confirmed by the exothermic effect noticed in the DSC curve at 161.48 °C. The third weigh loss of 58% along with an exothermic peak at 233.96 °C is caused by the degradation of the crystalline SnO_2 phase. The exothermic peaks in the range of 160-300 °C can initiate the ignition and then lead to self-propagation of the combustion reaction. At higher temperatures, above 500 °C, a slight weight loss corresponds to the decomposition of residual organic components.

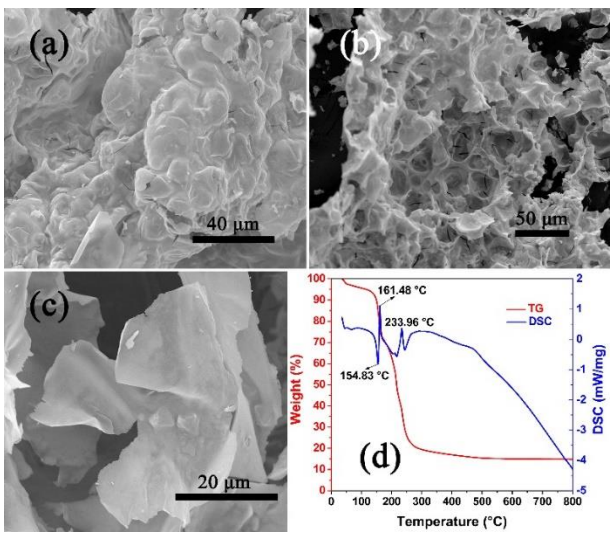

Fig. 2 (a, b) SEM images of both featured sides of pristine SnO_2, and (c) the representative high-magnification SEM image of SnO_2 sheets. (d) TGA-DSC curves of pristine SnO_2 synthesized by a solution combustion route.

Fig. 3 displays the SEM images of SnO_2 with different Pt functionalized contents (0 wt%, 0.5 wt%, 1 wt% and 2 wt%). As can be seen, no significant difference but more attached sheets than pristine SnO_2 is found, implying that Pt is not dominant factor for SnO_2 growth in our combustion synthesis process. The EDX pattern of 2 wt% Pt-functionalized SnO_2 reveals the constituent elements: Sn, O, and Pt (Fig. 3 (d)). It is worthwhile to note that the residual Cl element is also found by the content of 0.77 wt%. Meanwhile, the Pt content is 1.94 wt%, which is consistent with the experimental design.

Journal of Materials Chemistry A Accepted Manuscript

Details of pristine SnO_2 and 2 wt% Pt-SnO_2 have been further characterized by TEM and HRTEM. Fig. 4 (a) displays the TEM images of pristine SnO_2. It can be seen that the SnO_2 sheets consist of a large number of nanoparticles.

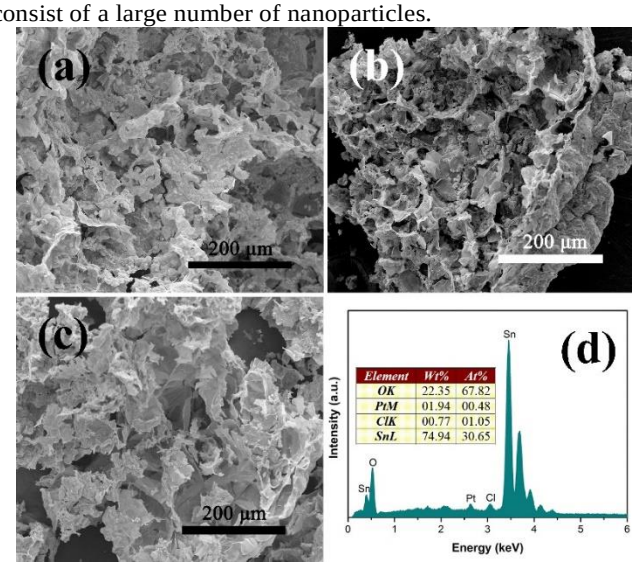

Fig. 3 SEM images of (a) 0.5 wt% Pt-SnO_2, (b) 1 wt% Pt-SnO_2, and (c) 2 wt% Pt-SnO_2, respectively. (d) EDX pattern of 2 wt% Pt-SnO_2.

From a high-magnification of TEM image in inset of Fig. 4 (a), the SnO_2 nanoparticles are irregular in size, up to tens of nanometers diameter, which is good agreement with the above estimated grain size from XRD results. Moreover, many pores are randomly distributed over the sheets owing to the inter-connected and loosely packed SnO_2 nanoparticles. Fig. 4 (b) shows a selected area electron diffraction pattern (SAED) of pristine SnO_2. From the inside to the outside, all diffraction rings on this SAED pattern are exactly assigned to the reflections (200), (101), (110), (211), and (112) of rutile SnO_2 phase, demonstrating that the as-synthesized SnO_2 sheets are polycrystalline, which agrees with the aforementioned XRD results. In regard to 2 wt% Pt-SnO_2, the sheet and nanoparticles are similar to pristine SnO_2, as revealed by TEM image in Fig. 4 (c). This porous sheet is believed to be favorable for gas sensors, which can facilitate the inward and outward gas diffusion.

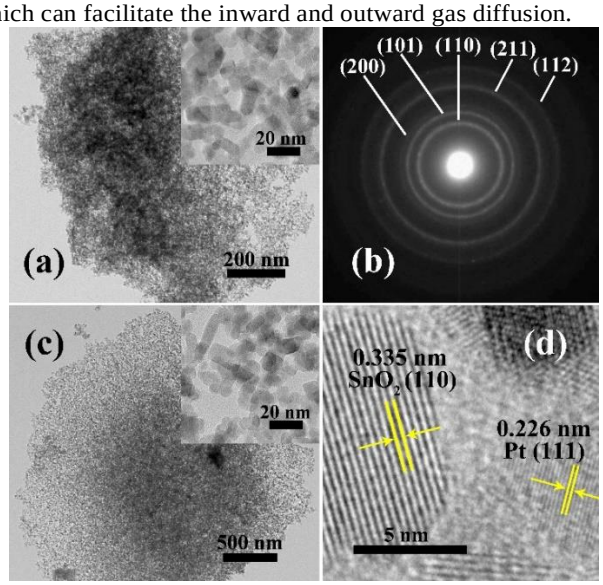

Fig. 4(a) TEM micrograph of pristine SnO_2 (inset shows the high-magnification of TEM image), and (b) a corresponding selected area electron diffraction pattern (SAED). (c) TEM micrograph of 2 wt% Pt-SnO_2 (inset displays the high-magnification of TEM image), and (d) the corresponding HRTEM image with obvious SnO_2 and Pt lattice fringes.

Note that the Pt nanoparticles are difficult to find because they disperse among SnO_2 nanoparticles with similar size. Fig. 4 (d) displays a HRTEM micrograph of 2 wt% Pt-SnO_2. The larger crystallite on the left of the micrograph shows lattice fringes with interplanar distance of 0.335 nm, which corresponds to the (110) plane of SnO_2. The smaller crystallite on the right of the micrograph displays the lattice fringes with interplanar distance of 0.226 nm, which corresponds to the (111) plane of Pt.No signs of PtO or PtO_2 phases are observed in many HRTEM micrographs of Pt-functionalized SnO_2, strongly supporting the above XRD measurements again. The high crystallinity of Pt-functionalized SnO_2 is beneficial for the long-term stability of the sensors.

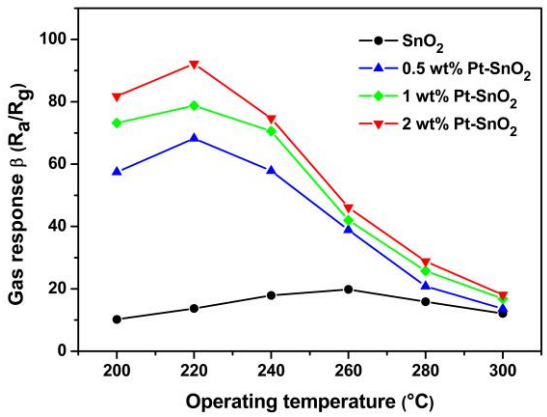

Fig. 5 IPA gas responses of as-synthesized SnO_2 with different Pt functionalization based sensors towards a gas concentration of 50 ppm at different operating temperature.

As is well known, the operating temperature range is an important characteristic for semiconducting oxide sensors. Hence, the temperature-dependence behavior and the optimal operating temperature of the gas sensors based on different Pt-functionalized SnO_2 to 50 ppm of IPA were firstly measured by varying the heating voltage to achieve the highest sensitivity. The obtained results are displayed in Fig. 5. It can be observed that as the temperature is increased, the responses initially increase gradually and then decrease with further increase of the operating temperature because of the achievement of maximum dynamic adsorption-desorption equilibrium.[2] At lower operating temperature, the sensitivity of gas sensors is quite low due to the lower adsorption of IPA and interaction between IPA gas molecules and sensing materials. With the temperature increase, a higher response is achieved due to the increase of active oxygen species such as O^-, O^{2-}, and O_2^- coming from the activation of both adsorbed molecular oxygen and lattice oxygen.[18] This tendency remains continuous up to a certain optimal temperature, surpassed when gas molecules begin to desorb in large quantities, resulting in an obvious drop in sensor response.[19] Therefore, the optimal operating temperature is at an equilibrium point between adsorption and desorption processes. The the largest response for the sensor based on pristine SnO_2 was exhibited at 260 °C with a value of 19.84. For gas sensors based on Pt functionalized SnO_2, the optimal operating temperatures decreased significantly to 220 °C. Also, the

Journal of Materials Chemistry A Accepted Manuscript

This journal is © The Royal Society of Chemistry 2012

response to 50 ppm of IPA was greatly increased by increasing the Pt functionalized level with the highest responses of 68.25, 78.74, and 92.21 for gas sensors based on 0.5, 1, and 2 wt% Pt-functionalized SnO_2 at 220 °C, respectively. These findings in turn directly verify the promoted effect of Pt functionalization. Hereinafter, we choose 220 °C as our operating temperature to proceed with the subsequent detections for different IPA concentrations in the range of 5-100 ppm.

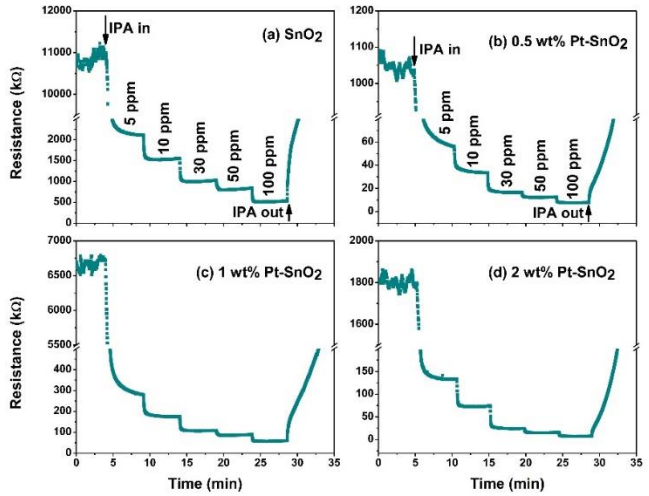

Fig. 6 Dynamic sensing curves of (a) pristine SnO_2, (b) 0.5 wt% Pt-SnO_2, (c) 1 wt% Pt-SnO_2, and (d) 2 wt% Pt-SnO_2 based on sensors to IPA in the range of 5-100 ppm at 220 °C.

The representative dynamic responses based on different contents of Pt-functionalized SnO_2 were investigated in detail. As shown in Fig. 6, all sensors showed fast and strong responses to IPA gas with concentrations ranging from 5 to 100 ppm at the optimal operating temperature of 220 °C. As can be noticed, all sensors displayed a reduced resistance upon exposure to IPA, as typically observed in n-type semiconductor gas sensors. Moreover, the sensor responses greatly increase with increasing IPA concentration and exhibit a lower detection limit of 5 ppm IPA regardless of Pt functionalized level.

The investigated sensor sensitivities as a function of IPA concentrations are summarily provided in Fig. 7. It can be seen that the Pt contents have a great influence on the responses of sensors for IPA detection in the range of 5 to 100 ppm at 220 °C. For example, the response to 5 ppm of IPA at 220 °C varied from 5.07 for the pristine SnO_2 sensor to 17.96, 21.51, and 25.92 for the Pt-functionalized SnO_2 sensors with Pt contents of 0.5, 1, and 2 wt%, respectively. Particularly, the response to 100 ppm IPA was greatly enhanced from 21.53 for the pristine SnO_2 sensor up to 190.50 for the 2 wt% Pt-SnO_2 sensor, corresponding to an almost 9-fold enhancement. This response value is higher than that of gas sensors based on SnO_2 nanorods,[20] and mixed phase of tetragonal and orthorhombic SnO_2 nanorods[2] to IPA at the same concentration. These results clearly demonstrate that the gas sensing properties of SnO_2 based sensor are significantly enhanced by Pt functionalization, in agreement with previous reports.[14-16]

In general, the sensing properties are strongly impacted by the specific surface area of the materials. Due to the almost identical morphologies and microstructures with or without Pt loading, we further checked the specific surface area of all samples. As shown in Fig. S3, the BET specific surface areas were measured to be 41.93, 36.45, 35.43, and 49.23 m^2/g for SnO_2, 0.5 wt%, 1 wt%, and 2 wt% Pt-SnO_2, respectively. No big difference of the specific surface areas with the different Pt contents are observed. Thus, we believe that the Pt loading is mainly reason for the significant enhancement in response.

The enhanced IPA sensing characteristics of the Pt-functionalized SnO_2 sheets might be ascribed to a number of possible reasons, including electron interactions between Pt nanoparticles and SnO_2, the catalytic promotion of the surface reaction with IPA by Pt nanoparticles (spillover effect), and the increase of oxygen species quantity on the surface of SnO_2.[21] Currently, the gas sensing mechanism of metal oxides like SnO_2 is understood by the change in the electrical resistance of metal oxides under different gas atmospheres. As depicted in Fig. S2 (Supp. Inf.), when the n-type SnO_2 based gas sensor is exposed to air, oxygen molecules will be chemisorbed and attract some electrons of SnO_2, hence inducing an electron depletion layer. As a result, the absorbed oxygen molecules are changed into active O_x^- ions such as O^-, O^{2-}, and O_2^- on the surface of SnO_2 by the following established chemical equilibrium:[22]

$$O_2 \overset{e}{\leftrightarrow} O_2^- \overset{e}{\leftrightarrow} O^- \overset{e}{\leftrightarrow} O^{2-} \qquad (2)$$

Upon exposure to reduction gases like IPA, the reduction reaction between O_x^- ions and IPA will occur above a certain temperature, thereby some oxygen species can be removed from the surface of SnO_2, leading to the release of the trapped electrons back into the conduction band to decrease the electron depletion layer, as depicted below:

$$IPA + O_x^- (O^-/O_2^-/O^{2-}) \rightarrow CO_2 + H_2O + e^- \quad (3)$$

Therefore the absorbed oxygen plays a critical role and the above process brings about the measureable variation of the resistance. Also, it was found that VOCs such as acetone, gasoline and formaldehyde gas can produce electrons at the same time as being decomposed to CO_2, and H_2O.[23]

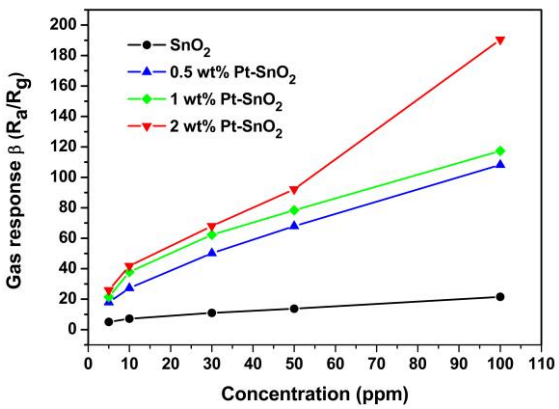

Fig. 7 Sensitivities of SnO_2 with different Pt functionalization based sensors towards various IPA concentrations at optimal operating temperature of 220 °C.

Noble-metal functionalization has been widely reported in previous literature to promote gas sensing performance.[24] To further understand the enhanced sensing performance through Pt nanoparticle functionalization, the surface state of 2 wt% Pt-SnO_2 was examined by XPS. The measured spectra surveys were decomposed into Gaussian components with a Shirley background using the software XPSPEAK. Fig. S4 displays the Sn 3d, O 1s and Pt 4f spectra of 2 wt% Pt-SnO_2. The Sn 3d doublet $3d_{3/2}$-$3d_{5/2}$ splitting peaks at 486.49 and 494.90 eV with better symmetry are investigated in Fig. S4 (a), and are assigned to the lattice tin in SnO_2. The binding energy difference of these two peaks is 8.48 eV, which is in good agreement with reported values for SnO_2. The characteristic peak of O 1s appears

Journal of Materials Chemistry A Accepted Manuscript

asymmetric (Fig. S4 (a)), which can be carefully deconvoluted into three peaks and assigned properly. The main peak centered at 530.23 eV is assigned to oxygen ions in the SnO_2 crystal lattice ($O_{lattice}$) under completely oxidized stoichiometric conditions,[25] whereas the peak located at 533.05 eV is attributed to adsorbates of oxygen. Importantly, the peaks located at 531.52 eV can be ascribed to the absorbed O_x^- species caused by oxygen vacancy (V_o), oxygen interstitial (O_i), and oxygen antisite [O_{Sn}],[26] which are able to interact with the IPA gas. Thus, the increasing number of adsorbed oxygen ions could contribute to gas sensitivity because that the lattice oxygen does not react with the reducing gas. As identified in Fig. S4 (c), the state of Pt 4f contains spin-orbital of Pt $4f_{7/2}$ and Pt $4f_{5/2}$ at 70.52 and 74.16 eV, respectively, which confirms the existence of Pt nanoparticles in 2 wt% Pt-SnO_2. Such observations also support the above XRD and TEM findings that no PtO and PtO_2 phases could be found. After Pt nanoparticles functionalization, the interaction between Pt and SnO_2 surfaces would occur (named electronic sensitization),[27] resulting in the change of Fermi level of SnO_2 or the work function of SnO_2, which favors the gas sensing performance. Under the assistance of functionalized Pt nanoparticles, the quantities of active O_x^- species are considerably enriched due to the easily adsorbed oxygen molecules and the facilitation of the conversion of oxygen molecules to O_x^- ions.[21] Furthermore, the oxidation of IPA molecules on the surface of SnO_2 might be catalyzed and enhanced under the activation of Pt nanoparticles via the spillover effect, which has been reported for SnO_2[14] and other oxide semiconductor based sensors.[27,28] Therefore, the response of the Pt-functionalized SnO_2 is distinctly enhanced compared to its pristine counterpart and further increases with the increase of Pt contents.

4. Conclusions

In conclusion, porous Pt-functionalized SnO_2 sheets were synthesized via a simple solution combustion method. The combusted precursor was composed of $SnCl_2{\cdot}2H_2O$, HNO_3, and $CO(NH_2)_2$ and the reaction was performed at temperature of 400 °C for 30 min. The obtained Pt-functionalized SnO_2 sheets are comprised of large number of SnO_2 nanoparticles ranging from several up to tens of nanometers in diameter. Compared with a pristine SnO_2 sheets based gas sensor, the Pt-functionalized SnO_2 based gas sensors showed lower operating temperatures and substantially enhanced responses to IPA gas with increasing Pt content. The gas response of the 2 wt% Pt-SnO_2 based gas sensor to 100 ppm IPA was 190.50, almost 9 times higher than that of the pristine SnO_2 counterpart. The enhancement of gas-sensing properties is attributed to considerably increased surface oxygen species, the electronic sensitization between Pt nanoparticles and SnO_2, and the catalytic oxidation promoted by Pt nanoparticles. We believe that these findings will not only render a novel route to synthesize SnO_2 nanostructures by solution combustion synthesis, but also provide Pt-functionalized SnO_2 materials for gas sensors for IPA detection with high responses.

Acknowledgements

This work was supported by National Natural Science Foundation of China (Grant No.51262029), the Department of Science and Technology of Yunnan Province via the Key Project for the Science and Technology (Grant No.2011FA001), the Key Project of the Department of Education of Yunnan Province (ZD2013006), and Program for Excellent Young Talents, Yunnan University. Igor Djerdj acknowledges financial support from the Unity through Knowledge Fund (www.ukf.hr) of the Croatian Ministry of Science, Education and Sports (Grant Agreement No. 7/13).

Notes and references

[a]Department of Materials Science and Engineering, Yunnan University, 650091 Kunming, Peoples' Republic of China. Fax: +86-871-65153832; Tel: +86-871-65031124; E-mail: ydwang@ynu.edu.cn.
[b]Ruđer Bošković Institute, Bijenička 54, 10000 Zagreb, Croatia. Fax: +38514680114; Tel: +38514680113; E-mail: igor.djerdj@irb.hr.

Electronic Supplementary Information (ESI) available: [Fig. S1. A schematic illustration of the preparation of porous SnO_2 sheets by a solution combustion synthesis and the assembling of the sensor; Fig. S2. Schematic diagram of the mechanism for IPA gas sensing; Fig. S3. The nitrogen adsorption-desorption isothermal curves; Fig. S4. The high-resolution XPS survey spectra of (a) Sn 3d, (b) O 1s, and (c) Pt 4f in 2 wt% Pt- SnO_2.]. See DOI: 10.1039/b000000x/

1. L. Francioso, A. Forleo, A. M. Taurino, P. Siciliano, L. Lorenzelli, V. Guarnieri, A. Adami and G. Agnusdei *Sens. Actuators B*, 2008, **134**, 660.
2. D. Hu, B. Q. Han, S. J. Deng, Z. P. Feng, Y. Wang, J. Popovic, M. Nuskol, Y. D. Wang and I. Djerdj, *J. Phys. Chem. C*, 2014, **118**, 9832.
3. S. Das and V. Jayaraman, *Prog. Mater. Sci*., 2014, **66**, 112.
4. K. Suematsu, Y. Shin, Z. Q. Hua, K. Yoshida, M.Yuasa, T. Kida and K. Shimanoe, *ACS Appl. Mater. Interface*, 2014, **6**, 5319.
5. Q. Kuang, C. S. Lao, Z. L. Wang, Z. X. Xie and L. S. Zheng, *J. Am. Chem. Soc*, 2007, **129**, 6070.
6. D. Wang, X. F. Chu and M. L. Gong, *Sens. Actuators B*, 2006, **117**, 183.
7. Z. J. Wang, Z. Y. Li, T. T. Jiang, X. R. Xu and C. Wang, *ACS Appl. Mater. Interfaces*, 2013, **5**, 2013.
8. J. J. Moore and H. J. Feng, *Prog. Mater. Sci.*, 1995, **39**, 243.
9. A. G. Merzhanov, *J. Mater. Chem*., 2004, **14**, 1779.
10. W. Wen, J. M. Wu, and Y. D. Wang, *Appl. Phys. Lett.*, 2012, **100**, 262111.
11. M. G. Kim, M. G. Kanatzidis, A. Facchetti and T. J. Marks, *Nat. Mater*., 2011, **10**, 382.
12. S. Bai, M. T. Cao, Y. Z. Jin, *et al.*, *Adv. Energy Mater*., 2014, **4**, 1301460.
13. J. H. Kang, J. Y. Kim and D. Y. Jeon, *J. Electrochem. Soc*., 2005, **152**, H33.
14. B. H. Jang, O. Landau, S. J. Chio, J. Shin, A. Rothschild and I. D. Kim, *Sens. Actuators B*, 2013, **188**, 156.
15. I. Kocemba and J. Rynkowski, *Sens. Actuators B*, 2011, **155**, 659.
16. X. Y. Xue, Z. H. Chen, C. H. Ma, L. L. Xing, Y. J. Chen and T. H. Wang, *J. Phys. Chem. C*, 2010, **114**, 3968.
17. A. R. Bueno, F. M. Oman, P. M. Jardim, N. A. Rey and R. R. Avillez, *Microporous Mesoporous Mater.*, 2014, **185**, 86.
18. Y. F. Sun, S. B. Liu, F. L. Meng, J. Y. Liu, Z. Jin, L. T. Kong and J. H. Liu, *Sensors*, 2012, **12**, 2610.
19. Z. M. Li, X. Y. Lai, H. Wang, D. Mao, C. J. Xing and D. Wang, *J. Phys. Chem. C*, 2009, **113**, 2792.

Journal of Materials Chemistry A Accepted Manuscript

 This journal is © The Royal Society of Chemistry 2012

20. D. Hu, B. Q. Han, R. Han, S. J. Deng, Y. Wang, Q. Li and Y. D. Wang, *New J. Chem*., 2014, **38**, 2443.
21. N. Yamazoe, Y. Kurokawa and T. Seiyama, *Sens. Actuators B*, 1983, **4**, 283.
22. S. P. Xu, F. Q. Sun, F. L. Gu, Y. B. Zuo, L. H. Zhang, C. F. Fang, S. M. Yang and W. S. Li, *ACS Appl. Mater. Interfaces*, 2014, **6**, 1251.
23. T. Chen, Q. J. Liu, Z. L. Zhou and Y. D. Wang, *Sens. Actuators B*, 2008, **131**, 3021.
24. Y. F. Sun, S. B. Liu, F. L. Meng, J. F. Liu, Z. Jin, L. T. Kong and J. H. Liu, *Sensors*, 2012, **12**, 2610.
25. Y. D. Wang, I. Djerdj, M. Antonietti and B. M. Smarsly, *Small*, 2008, **4**, 1656.
26. M. Chen, Z. Wang, D. Han, F. Gu and G. Guo, *J. Phys. Chem. C*, 2011, **115**, 12763.
27. J. C. Fu, C. H. Zhao, J. L. Zhang, Y. Peng and E. Q. Xie, *ACS Appl. Mater. Interfaces*, 2013, **5**, 7410.
28. X. H. Liu, J. Zhang, T. L. Yang, X. Z. Guo, S. H. Wu and S. R. Wang, *Sens. Actuators B*, 2011, **156**, 918.

Journal of Materials Chemistry A Accepted Manuscript